

NMR Search for the Spin Nematic State in LaFeAsO Single Crystal

M. Fu¹, D. A. Torchetti¹, T. Imai^{1,2}, F.L. Ning³, J.-Q. Yan^{4,5,6}, and A. S. Sefat⁴

¹*Department of Physics and Astronomy, McMaster University, Hamilton, Ontario L8S4M1, Canada*

²*Canadian Institute for Advanced Research, Toronto, Ontario M5G1Z8, Canada*

³*Department of Physics, Zhejiang University, Hangzhou 310027, China*

⁴*Materials Science and Technology Division, Oak Ridge National Laboratory, TN 37831, USA*

⁵*Department of Materials Science and Engineering,*

The University of Tennessee at Knoxville, Knoxville, TN 37996, USA and

⁶*Division of Materials Science and Engineering, Ames Laboratory, US-DOE, Ames, Iowa 50011, USA*

(Dated: October 15, 2018)

We report a ⁷⁵As single crystal NMR investigation of LaFeAsO, the parent phase of a pnictide high T_c superconductor. We demonstrate that spin dynamics develop a strong two-fold anisotropy within each orthorhombic domain below the tetragonal-orthorhombic structural phase transition at $T_{TO} \approx 156$ K. This intermediate state with a dynamical breaking of the rotational symmetry freezes progressively into a spin density wave (SDW) below $T_{SDW} \approx 142$ K. Our findings are consistent with the presence of a spin nematic state below T_{TO} with an incipient magnetic order.

PACS numbers: 74.70.Xa, 76.60.-k

The mechanism of high T_c superconductivity in iron pnictides remains enigmatic [1]. Earlier NMR measurements demonstrated that low frequency spin fluctuations associated with the spin density wave (SDW) instability grow toward T_c near optimal doping [2–5], favoring the scenario of spin-fluctuation induced superconductivity. There is, however, a complication; the slowing of the lattice vibrations accompanies that of spin fluctuations [6–8]. For example, neutron scattering measurements showed that LaFeAsO undergoes a tetragonal-orthorhombic structural phase transition at $T_{TO} \approx 156$ K, followed by a SDW ordering at $T_{SDW} \approx 142$ K [6, 9, 10]. Moreover, the softening of the lattice begins at as high as ~ 200 K, and continues through T_{TO} and T_{SDW} down to $T_{Domains} \approx 120$ K [6], where the growth of the orthorhombic domains ends [10, 11]. Theoretical analysis of LaFeAsO based on the frustrated J_1 - J_2 model suggests that the Ising symmetry of Fe spins may be already broken below T_{TO} without a three-dimensional magnetic long-range order [12]. Moreover, the intermediate temperature range between T_{TO} and T_{SDW} of LaFeAsO may be identified as a *spin nematic state* [13].

In such a nematic state, the spin correlations break the tetragonal symmetry, i.e. $\langle \mathbf{S}_i \cdot \mathbf{S}_{i+x} \rangle = -\langle \mathbf{S}_i \cdot \mathbf{S}_{i+y} \rangle$ (we refer readers to Fig. 1 of a review article [14] for a pictorial demonstration of the nematic state). More recent theoretical analysis based on an itinerant electron picture [15] or an orbital fluctuation model [16] also led to analogous conclusions. The prospect of observing such a magnetic analogue of a liquid crystal below T_{TO} with an incipient (“fluctuating”) magnetic order, and its potential link with the mechanism of high T_c superconductivity, has stimulated strong interest among researchers. The past experimental efforts searching for the signature of nematicity were focused primarily on the BaFe₂As₂ series (e.g. [17–20]). However, the proximity between the structural and SDW transitions, and/or the twinning of orthorhombic domains hampered these efforts.

In this Letter, we report a microscopic ⁷⁵As NMR investigation of LaFeAsO for a single crystal [21], and compare our results with neutron scattering [10] and magnetic susceptibility χ measured for the same piece of ~ 20 mg crystal. The usage of a single crystal enabled us to resolve complicated changes of NMR lineshapes across T_{TO} and T_{SDW} for the first time, and find the signature of the spontaneous breaking of the rotational symmetry. We will demonstrate that low frequency spin dynamics indeed exhibit a strong anisotropy within *each* orthorhombic domain with a two-fold symmetry below $T_{TO} \approx 156$ K. Moreover, the anisotropic spin state freezes progressively into a static SDW from $T_{SDW} \approx 142$ K to $T_{Domains} \approx 120$ K, and the SDW ordered and paramagnetic domains coexist in a broad range of temperature. Our findings uncover the presence of an unconventional intermediate spin state below T_{TO} with the signatures of spin nematicity.

In Fig. 1, we summarize representative field-swept ⁷⁵As NMR lineshapes observed at $f_{NMR} = 58.159$ MHz (nuclear spin $I = 3/2$). When we apply an external magnetic field B_{ext} along the c-axis, a sharp paramagnetic (PM) *central peak* appears at $B_{ext}^{center} \sim 7.96$ T for the $I_z = +1/2$ to $-1/2$ transition, as shown in Fig. 1(b); the resonant condition is $f_{NMR} = (1 + {}^{75}K)\gamma_n B_{ext}^{center}$, where the nuclear gyromagnetic ratio $\gamma_n/2\pi = 7.2919$ MHz/T. ${}^{75}K \sim 0.002$ ($\sim 0.2\%$) is the Knight shift, which measures the product between the local spin susceptibility and the hyperfine coupling constant. We note that the full-width at half-maximum of the PM central peak is as sharp as 6.5 kHz (8.9 Oe) at 290 K in the absence of orthorhombic distortion. The narrow linewidth is comparable to that of undoped BaFe₂As₂ [22, 23], and attests to the high homogeneity of our crystal.

In Fig. 1(a), we observe an $I_z = \pm 3/2$ to $\pm 1/2$ paramagnetic *satellite peak* near $B_{ext}^{satellite} = 6.7$ T (connected by a dotted line). We also found the strongly temperature dependent antiferromagnetic (AF) central peak aris-

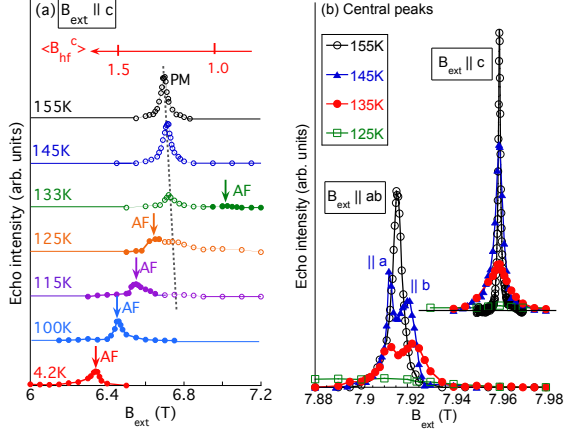


FIG. 1: (Color online) Representative ^{75}As NMR lineshapes observed at 58.159 MHz. (a) The paramagnetic (PM) satellite peak (\circ), and the antiferromagnetic (AF) central peak marked with a downward arrow (\bullet) in $B_{ext} \parallel c$. For clarity, the vertical axis is shifted for different temperatures. The dotted line indicates the shift of the PM satellite peak with temperature. The horizontal axis at the top of (a) measures the split $\langle B_{hf}^c \rangle$ from the PM central peak at 7.96 T in (b). (b) The PM central peak with $B_{ext} \parallel c$ (upper right) and $B_{ext} \parallel ab$ (lower left). For clarity, the origin of the vertical axis is shifted for $B_{ext} \parallel c$. The formation of twinned orthorhombic domains along the two orthogonal axes, as schematically shown in Fig. 2(a), results in the splitting of the $B_{ext} \parallel ab$ lineshape below $T_{TO} \approx 156$ K.

ing from the statically SDW ordered domains (marked by downward arrows), but only below the onset temperature of $T_{SDW}^{NMR} \approx 135$ K ($< T_{SDW}$). The AF central peak is shifted from the PM central peak at $B_{ext}^{center} \sim 7.96$ T in Fig. 1(b) by a static hyperfine field along the c -axis, $\langle B_{hf}^c \rangle$. $\langle B_{hf}^c \rangle$ originates from the ordered Fe magnetic moments M_{Fe} , and $\langle B_{hf}^c \rangle \propto M_{Fe}$ [22]. In Fig. 2(b), we deduce the temperature dependence of $\langle B_{hf}^c \rangle$ from Fig. 1(a), and compare the results with the neutron scattering data of M_{Fe} [10].

The splitting between the central and satellite peaks, $\nu_Q^c = \gamma_n(B_{ext}^{center} - B_{ext}^{satellite}) \approx 9.2$ MHz, measures the nuclear quadrupole interaction with the electric field gradient (EFG). We summarize the temperature dependence of ν_Q^c in Fig. 2(c). The EFG is the second derivative of the Coulomb potential arising from electrons and ions near the observed ^{75}As sites. Below $T_{TO} \approx 156$ K, ν_Q^c exhibits a sharp downturn, because the EFG is sensitive to the local structural environment. Earlier diffraction measurements showed that the growth of orthorhombic domains finally comes to an end at $T_{Domains} \approx 120$ K [10, 11]; ν_Q^c also levels off below $T_{Domains}$.

In Fig. 1(b), we also show representative NMR lineshapes with B_{ext} applied along the tetragonal a -axis within the FeAs planes. Above T_{TO} , all tetragonal domains are equivalent, hence we observe a single central

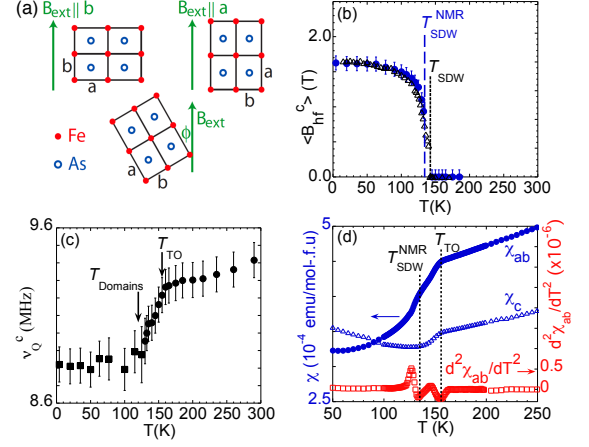


FIG. 2: (Color online) (a) Schematics of the orthorhombic domain with $B_{ext} \parallel b$ (upper left) and $B_{ext} \parallel a$ (upper right) within twinned ab -planes. Bottom: rotation by azimuthal angle ϕ . (b) (\bullet): $\langle B_{hf}^c \rangle$ deduced from Fig. 1(a). (Δ): the sub-lattice magnetization M_{Fe} deduced as the square-root of the magnetic Bragg scattering intensity (after ref.[10]), normalized at 4.2 K. (c) ν_Q^c measured for the paramagnetic (\bullet) and antiferromagnetic (\blacksquare) peaks. (d) The magnetic susceptibility χ_{ab} (\bullet) and χ_c (Δ) measured in 1 T with dc-SQUID. Also shown is the second derivative of χ_{ab} (\square). Notice the presence of two kinks in χ_{ab} at ~ 156 K and ~ 133 K, as evidenced by the negative maxima of $d^2\chi_{ab}/dT^2$.

peak. Below T_{TO} , the elongated a -axis of each domain points either along the direction of B_{ext} , or orthogonal to B_{ext} , due to twinning of the orthorhombic domains, as sketched in Fig. 2(a). Moreover, orthorhombic distortion breaks the axial symmetry of the EFG. The difference in the second order effects of the nuclear quadrupole interaction thus results in splitting of the central peak; the peak positions depend on the direction of the elongated a -axis relative to B_{ext} . We confirmed that the NMR line splitting in Fig. 1(b) is caused entirely by the difference in the second order nuclear quadrupole effects, which is inversely proportional to B_{ext} [24]. That is, the NMR Knight shift is still axially symmetric, and shows very little temperature dependence below T_{TO} , $^{75}K_a = ^{75}K_b \approx 0.22 \pm 0.03$ %. In view of the fact that expansion of the lattice from T_{TO} to 290 K results in a larger value of the quadrupole frequency as shown in Fig. 2(c), we tentatively assign the peak near $B_{ext} \sim 7.91$ T to the orthorhombic domains with $B_{ext} \parallel a$; the other peak near $B_{ext} \sim 7.92$ T arises from the orthorhombic domains with $B_{ext} \parallel b$ instead. From the splitting of an $I_z = \pm 3/2$ to $\pm 1/2$ satellite peak, we estimate $\nu_Q^a \sim 5.2$ MHz and $\nu_Q^b \sim 3.9$ MHz at 145 K. We also confirmed that these double peaks collapse into one when we apply B_{ext} along the $[110]$ direction within the ab -plane, because B_{ext} points along the diagonal direction for all orthorhombic domains in such a geometry.

For bulk averaged measurement techniques such as re-

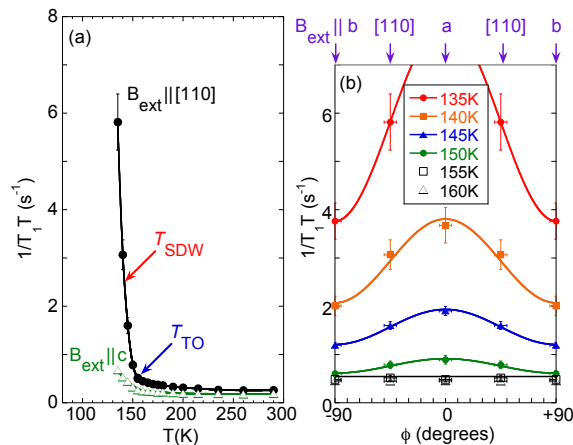


FIG. 3: (Color online) (a) Temperature dependence of $1/T_1T$ measured for the PM central peak with B_{ext} along the [110] (●), and the c-axis (△) direction. The solid curves are guides to the eye only. (b) $1/T_1T$ as a function of the field orientation ϕ as defined in Fig. 2(a), within each orthorhombic domain. The results are symmetrized for $\phi \leq 0$ due to crystal symmetry. Below $T_{TO} \sim 156$ K, $1/T_1T$ exhibits increasingly strong dependence on the in-plane orientation of B_{ext} , which can be modeled by the function $1/T_1T = A + B \cos^2 \phi$ (solid curves). The accidental superposition between different NMR peaks makes accurate measurements of $1/T_1T$ unfeasible below 135-140 K, depending on the direction of B_{ext} .

sistivity, the twinning of orthorhombic domains would result in experimental data averaged over two orthogonal directions within the ab-plane, unless one applies a uniaxial stress [17–20]. It is not straightforward, then, to probe the *spontaneous* breaking of the rotational symmetry. In contrast, NMR is a local probe. Since we have succeeded in resolving the central peaks in Fig. 1(b) for different orientations, we can investigate the in-plane anisotropy of spins within each orthorhombic domain.

In Fig. 3(a), we summarize the temperature dependence of the nuclear spin-lattice relaxation rate $1/T_1$ divided by T , $1/T_1T$, for the PM central peaks [25]. Our preliminary $1/T_1T$ results for the SDW ordered state are very similar to the case of $BaFe_2As_2$ [22], and beyond the scope of the present work. $1/T_1T$ measures low-frequency spin fluctuations: $(1/T_1T)_\alpha \propto \sum_{\mathbf{q}} |F(\mathbf{q})|^2 \chi''(\mathbf{q}, f_{NMR}) / f_{NMR}$, where α specifies the direction of B_{ext} , $|F(\mathbf{q})|^2$ and χ'' are the hyperfine form factor [26] and the imaginary part of the dynamical electron spin susceptibility, respectively, and the \mathbf{q} summation is taken within the Brillouin zone. $1/T_1T$ shows a mild increase with decreasing temperature down to T_{TO} due to the slow growth of a short range SDW order. Once we enter the orthorhombic phase below T_{TO} , $1/T_1T$ measured with $B_{ext} \parallel [110]$, a-, and b-axis begins to show rapid growth. This implies that the orthorhombic distortion enhances low frequency components of antiferromagnetic spin fluctuations, and that the dynamic SDW is rapidly slowing down [3, 23, 27]. This conclusion is consistent

with the downturn of χ below T_{TO} [6], also observed for our crystal as shown in Fig. 2(d). At first glance, the enhancement of $1/T_1T$ below T_{TO} is much weaker with $B_{ext} \parallel c$. This is simply because the transferred hyperfine fields at ^{75}As sites from their four nearest-neighbor Fe sites are geometrically cancelled out within the ab-plane in this configuration, i.e. $|F(\mathbf{Q})|^2 = 0$ for the SDW ordering wave vectors \mathbf{Q} , and the contributions of AF spin fluctuations to $(1/T_1T)_c$ are “filtered out” [26]. The growing anisotropy of $1/T_1T$ between the ab- and c-axis orientations observed below T_{TO} therefore has little to do with that of the critical dynamics of Fe spins near T_{SDW} .

Next, let’s turn attention to the angular dependence of $1/T_1T$ within the ab-plane, which has been proposed as a novel probe of spin nematicity [26]. As summarized in Fig. 3(b), we don’t observe any ϕ -dependence of $1/T_1T$ above T_{TO} . Once we enter the orthorhombic phase below T_{TO} , $1/T_1T$ begins to develop a strong anisotropy within each orthorhombic domain. The anisotropy reaches as much as a factor of ~ 2 by $\lesssim 140$ K. In view of the very small difference between the lattice constants of the a- and b-axis ($\sim 0.5\%$) [9, 10, 21], our finding is quite unexpected for paramagnetic spin fluctuations.

As explained above, the Knight shift remains axially symmetric within experimental uncertainties below T_{TO} . It is therefore unlikely that the uniform spin susceptibility or the hyperfine form factor $|F(\mathbf{q})|^2$ develops a sizable anisotropy within the ab-plane below T_{TO} . We therefore conclude that low frequency Fe spin dynamics as reflected in $\chi''(\mathbf{q}, f_{NMR})$ locally develop a strong rotational anisotropy by a factor of ~ 2 within *each* orthorhombic domain below T_{TO} , without exhibiting a three-dimensional magnetic order. We note that the intensities of the a- and b-peaks in Fig. 1(b) are comparable, hence FeAs planes are randomly twinned. When averaged over the entire single crystal, Fe spin dynamics would appear almost isotropic within the ab-plane.

The anomalous behavior of Fe spins below T_{TO} is not limited to the in-plane anisotropy of their dynamics. In Fig. 4, we summarize the temperature dependence of the integrated intensities of the NMR signal. An unusual aspect of the signal intensity is that the paramagnetic NMR peaks don’t disappear suddenly at $T_{SDW} \approx 142$ K, and linger well below T_{SDW} down to $T_{Domains} \approx 120$ K. On the other hand, AF NMR signals from statically SDW ordered domains emerge progressively, only below $T_{SDW}^{NMR} \approx 135$ K ($< T_{SDW}$). Notice that the PM central peak is still clearly observable below T_{SDW} in Fig. 1(b). Our finding that the PM signal intensity is as large as $\sim 60\%$ at T_{SDW}^{NMR} implies that $\sim 60\%$ of the sample volume remains paramagnetic at 135 K. That is, AF and PM domains coexist even below T_{SDW}^{NMR} , although neutron scattering begins to detect magnetic Bragg peaks below T_{SDW} [10]. In addition, $1/T_1T$ measured for the residual PM peak does not blow up at T_{SDW} , and continues to increase. If the SDW ordering in our LaFeAsO single crystal was a typical second order phase transition, $1/T_1T$ would diverge at T_{SDW} due to the critical

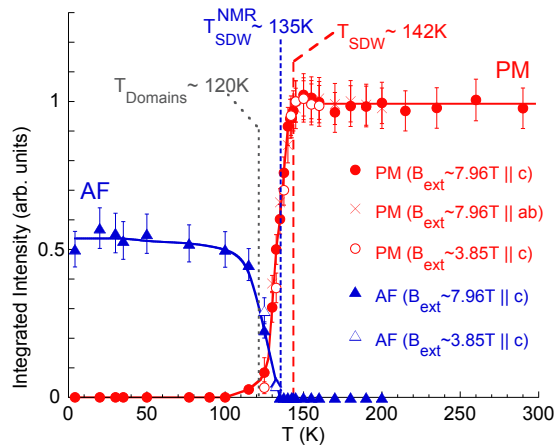


FIG. 4: (Color online) The temperature dependence of the PM and static AF volume fractions at the NMR time scale, measured as the integrated intensity of the PM and AF central peaks (normalized by the Boltzmann factor). The solid curves are guides to the eye. Notice that the PM phase coexists with the AF phase even below T_{SDW} down to $T_{Domains}$. We measured the spin echo with a delay time $2\tau = 40 \mu\text{s}$; the transverse relaxation time T_2 for the observable NMR signals is always long ($\sim\text{msec}$), and does not appreciably affect the intensity. Notice that lowering B_{ext} from $\sim 7.96 \text{ T}$ to $\sim 3.85 \text{ T}$ does not alter the qualitative features.

slowing down of spin fluctuations, followed by a sudden disappearance of PM NMR signals below T_{SDW} .

The reason NMR and neutron scattering detect different onset temperatures of the SDW is that each experimental probe has a different characteristic measurement time scale [28, 29]. Elastic neutron scattering measurements would consider the SDW ‘static’ when fluctuations slow down to below the instrument resolution of $\sim 1\text{meV}$. This means that neutron scattering can take an instantaneous picture of Fe spins with a ‘shutter speed’ of $\sim 10^{-11}$ sec even if they are still slowly fluctuating. In contrast, AF NMR signals in Fig. 1(a) become observable only when Fe spins in the SDW become static, to the extent that $\langle B_{hf}^c \rangle$ is time-independent over the duration of our spin echo measurements, $40 \mu\text{sec}$. If Fe moments are fluctuating faster than $40 \mu\text{sec}$ in some segments of FeAs planes, NMR would see them as motionally averaged out (i.e. paramagnetic). In other words, the different onset temperatures of the SDW ordering between neutron and NMR data indicate that the fluctuations of the SDW continue to slow down from $T_{SDW} \approx 142 \text{ K}$ to $T_{SDW}^{NMR} \approx 135 \text{ K}$. The coexistence of PM and AF domains below 142 K implies that the fluctuation time scales have a broad distribution throughout the FeAs planes. We also found that χ_{ab} exhibits an additional kink at $\sim 133 \text{ K}$, as shown in Fig. 2(d). Since SQUID measures the time-independent response of spins, the acceleration in the suppression of χ_{ab} below T_{SDW}^{NMR} is consistent with NMR.

It is interesting to realize that these unusual behav-

iors of LaFeAsO share similarities with the spin stripes in high T_c cuprates [30], where the concept of nematicity was originally proposed for unconventional superconductors [31]. In the striped cuprates, the spin stripes progressively slow down below a charge ordering at $\sim 70 \text{ K}$ [30] (instead of T_{TO}); elastic neutron scattering, μSR , and NMR detect the emergence of a static SDW at their respective measurement time scale below $\sim 50 \text{ K}$ [30], $\sim 30 \text{ K}$ [32], and $\sim 1.6 \text{ K}$ [28], respectively. Moreover, PM NMR signals linger well below $\sim 50 \text{ K}$ [28].

The temperature dependence of the AF NMR signal intensity in Fig. 4 indicates that the volume fraction of the static SDW at the time scale of NMR gradually increases from $T_{SDW}^{NMR} \approx 135 \text{ K}$ toward $T_{Domains} \approx 120 \text{ K}$. Once the growth of the orthorhombic domains ends at $T_{Domains}$ [10, 11], the intensity saturates at $\sim 60\%$ of the paramagnetic intensity above T_{SDW} . The missing signal intensity suggests that $\langle B_{hf}^c \rangle$ is still modulating and/or T_2 is too fast for a spin echo NMR signal to form in $\sim 40\%$ of the sample volume. Our finding is consistent with the earlier μSR measurements for a powder sample of LaFeAsO; the muon precession with a well-defined frequency of $\sim 23 \text{ MHz}$ takes place only in $\sim 70\%$ of the sample volume, and $\sim 30\%$ of the μSR signal is strongly damped [33]. It remains to be seen whether these ultra slow dynamics of the SDW in $30\text{-}40\%$ of the sample volume are caused by the motion of the anti-phase domain boundaries [29] and/or the finite size effects of the orthorhombic domains.

To summarize, we demonstrated that Fe spin fluctuations in a LaFeAsO single crystal begin to slow down below $T_{TO} \approx 156 \text{ K}$, accompanied by the local breakdown of the rotational symmetry of spin fluctuations in each of the randomly twinned orthorhombic domains. The way that the static SDW develops is also unconventional. The paramagnetic and SDW ordered domains coexist in a wide range of temperature below $T_{SDW} \approx 142 \text{ K}$ due to a distribution in the fluctuation time scales of the SDW. A large volume of FeAs planes sees freezing of the static SDW only below $T_{Domains} \approx 120 \text{ K}$. Our findings point towards the presence of a novel spin state between T_{TO} and $T_{Domains}$ with a dynamically broken rotational symmetry and an incipient magnetic order, i.e. the elusive *spin nematic state*.

The work at McMaster was supported by NSERC and CIFAR. The work at Zhejiang was supported by National Basic Research Program of China (No.2011CBA00103) and NSF of China (No. 11274268). Research at ORNL was supported by the Department of Energy, Basic Energy Sciences, Materials Sciences and Engineering Division. TI acknowledges helpful discussions with K. Ishida, H. Eisaki, S. Uchida, I. Mazin, J. Tranquada, B. Buechner, P. Canfield, and B. Gaulin. JQY thanks B. Jensen, K. Dennis, R. McCallum, and T. Lograsso for their assistance in crystal growth, which was also supported by the U.S. DOE.

-
- [1] Y. Kamihara, T. Watanabe, M. Hirano, and H. Hosono, *J. Amer. Chem. Soc.* **130**, 3296 (2008).
- [2] Y. Nakai, K. Ishida, Y. Kamihara, M. Hirano, and H. Hosono, *J. Phys. Soc. Jpn.* **77**, 073701 (2008).
- [3] F. L. Ning, K. Ahilan, T. Imai, A. S. Sefat, M. A. McGuire, B. C. Sales, D. Mandrus, P. Cheng, B. Shen, and H.-H. Wen, *Phys. Rev. Lett.* **104**, 037001 (2010).
- [4] G. Lang, H.-J. Grafe, D. Paar, F. Hammerath, K. Manthey, G. Behr, J. Werner, and B. Buchner, *Phys. Rev. Lett.* **104**, 097001 (2010).
- [5] T. Oka, Z. Li, S. Kawasaki, G. F. Chen, N. L. Wang, and G. Q. Zheng, *Phys. Rev. Lett.* **108**, 047001 (2012).
- [6] M. McGuire, A. Christianson, A. Sefat, B. C. Sales, M. D. Lumsden, R. Jin, E. A. Payzant, D. Mandrus, Y. Luan, V. Keppens, et al., *Phys. Rev. B* **78**, 094517 (2008).
- [7] R. M. Fernandes, L. H. VanBebber, S. Bhattacharya, P. Chandra, V. Keppens, D. Mandrus, M. A. McGuire, B. C. Sales, A. S. Sefat, and J. Schmalian, *Phys. Rev. Lett.* **105**, 157003 (2010).
- [8] M. Yoshizawa, D. Kimura, T. Chiba, A. Ismayil, Y. Nakanishi, K. Kihou, C. H. Lee, A. Iyo, H. Eisaki, M. Nakajima, et al., *J. Phys. Soc. Jpn.* **81**, 024604 (2012).
- [9] C. de la Cruz, Q. Huang, J. W. Lynn, J. Li, W. Ratcliff, J. L. Zarestky, H. A. Mook, G. F. Chen, J. L. Luo, N. L. Wang, et al., *Nature* **453**, 899 (2008).
- [10] H.-F. Li, W. Tian, J.-Q. Yan, J. L. Zarestky, R. W. McCallum, T. A. Lograsso, and D. Vaknin, *Phys. Rev. B* **82**, 064409 (2010).
- [11] A. Ricci, N. Poccia, B. Joseph, L. Barba, G. Arrighetti, G. Ciasca, J.-Q. Yan, R. W. McCallum, T. A. Lograsso, N. D. Zhigadlo, et al., *Phys. Rev. B* **82**, 144507 (2010).
- [12] C. Xu, M. Muller, and S. Sachdev, *Phys. Rev. B* **78**, 020501R (2008).
- [13] C. Fang, H. Yao, W. F. Tsai, J. P. Hu, and S. A. Kivelson, *Phys. Rev. B* **77**, 224509 (2008).
- [14] R. M. Fernandes and J. Schmalian, *Supercond. Sci. and Technol.* **25**, 084005 (2012).
- [15] R. M. Fernandes, A. V. Chubukov, J. Knolle, I. Eremin, and J. Schmalian, *Phys. Rev. B* **85**, 024534 (2012).
- [16] H. Kontani, T. Saito, and S. Onari, *Phys. Rev. B* **84**, 024528 (2011).
- [17] J.-H. Chu, J. G. Analytis, K. D. Greve, P. L. McMahon, Z. Islam, Y. Yamamoto, and I. R. Fisher, *Science* **329**, 824 (2011).
- [18] M. A. Tanatar, E. C. Blomberg, A. Kreyssig, M. G. Kim, N. Ni, A. Thaler, S. L. Budko, P. C. Canfield, A. I. Goldman, I. Mazin, et al., *Phys. Rev. B* **81**, 184508 (2010).
- [19] C. Dhital, Z. Yamani, W. Tian, J. Zarestky, A. S. Sefat, Z. Wang, R. J. Birgeneau, and S. D. Wilson, *Phys. Rev. Lett.* **108**, 087001 (2012).
- [20] M. Nakajima, S. Ishida, Y. Tomioka, K. Kihou, C. H. Lee, A. Iyo, T. Ito, T. Kakeshita, H. Eisaki, and S. Uchida, arXiv:1208.1581.
- [21] J.-Q. Yan, S. Nandi, J. L. Zarestky, W. Tian, A. Kreyssig, B. Jensen, A. Kracher, K. W. Dennis, R. J. McQueeney, A. I. Goldman, et al., *Appl. Phys. Lett.* **95**, 222504 (2009).
- [22] K. Kitagawa, N. Katayama, K. Ohgushi, M. Yoshida, and M. Takigawa, *J. Phys. Soc. Jpn.* **77**, 114709 (2008).
- [23] F. L. Ning, K. Ahilan, T. Imai, A. S. Sefat, R. Jin, M. A. McGuire, B. C. Sales, and D. Mandrus, *J. Phys. Soc. Jpn.* **78**, 013711 (2009).
- [24] M. Takigawa, P. C. Hammel, R. H. Heffner, Z. Fisk, J. L. Smith, and R. B. Schwarz, *Phys. Rev. B* **39**, 300 (1989).
- [25] See Supplemental Materials for examples of the T_1 recovery curves and their fit to the standard solution to the rate equation.
- [26] A. Smerald and N. Shannon, *Phys. Rev. B* **84**, 184437 (2011).
- [27] Y. Nakai, S. Kitagawa, T. Iye, K. Ishida, Y. Kamihara, M. Hirano, and H. Hosono, *Phys. Rev. B* **85**, 134408 (2012).
- [28] A. W. Hunt, P. M. Singer, A. F. Cederstrom, and T. Imai, *Phys. Rev. B* **64**, 134525 (2001).
- [29] I. Mazin and M. Johannes, *Nature Physics* **5**, 141 (2009).
- [30] J. M. Tranquada, B. J. Sternlieb, J. D. Axe, Y. Nakamura, and S. Uchida, *Nature* **375**, 561 (1995).
- [31] S. A. Kivelson, E. Fradkin, and V. J. Emery, *Nature* **393**, 550 (1998).
- [32] B. Nachumi, Y. Fudamoto, A. Keren, K. M. Kojima, M. Larkin, G. M. Luke, J. Merrin, O. Tchernyshyov, Y. J. Uemura, N. Ichikawa, et al., *Phys. Rev. B* **58**, 8760 (1998).
- [33] H. H. Klauss, H. Luetkens, R. Klingeler, C. Hess, F. J. Litterst, M. Kraken, M. M. Korshunov, I. Eremin, S. L. Drechsler, R. Khasanov, et al., *Phys. Rev. Lett.* **101**, 077005 (2008).